Earth, Planets and Space

EXPRESS LETTER

Open Access

Thick slab crust with rough basement weakens interplate coupling in the western Nankai Trough

Ryuta Arai[1*], Kazuya Shiraishi[1], Yasuyuki Nakamura[1], Gou Fujie[1], Seiichi Miura[1], Shuichi Kodaira[1], Dan Bassett[2], Tsutomu Takahashi[1], Yuka Kaiho[1], Yohei Hamada[3], Kimihiro Mochizuki[4], Rie Nakata[4,5], Masataka Kinoshita[4], Yoshitaka Hashimoto[6] and Kyoko Okino[7]

Abstract

The westernmost Nankai Trough, southwest Japan, exhibits a rapid along-strike reduction in plate coupling in the proximity to the subducting Kyushu-Palau ridge. Yet how and to what extent the ridge subduction impacts physical properties at the megathrust have not been investigated. Here we present high-resolution seismic P-wave velocity models along the forearc wedge in the western Nankai Trough derived from full-waveform inversion analyses of seismic refraction data. The velocity models show that where the plate coupling is weak and the plate boundary presumably hosts slow earthquakes, the upper plate exhibits lower seismic velocities indicating higher degree of fracturing over a ~ 100 km length along trough. Intriguingly, the extent of the upper-plate low-velocity features is significantly larger than the surficial width of the Kyushu-Palau ridge, and this low-velocity zone is underthrust by the slab with increased crustal thickness by 2–4 km. Seismic reflection images consistently reveal that the thicker slab crust has appreciable basement roughness extending ~ 60 km from the eastern margin of the Kyushu-Palau ridge beneath the western Shikoku basin. We suggest that such a thicker and rugged slab crust, together with the main body of the Kyushu-Palau ridge, can cause significant fracture zones in the overriding plate, decrease the interplate coupling and produce preferable conditions for shallow slow earthquakes to occur when subducted. The results may also provide structural constraints on the western limit of future megathrust earthquakes in the Nankai Trough.

Keywords Hyuga-nada, Seamount subduction, Kyushu-Palau ridge, Full-waveform inversion, Slow earthquakes, Plate coupling

*Correspondence:
Ryuta Arai
ryuta@jamstec.go.jp
Full list of author information is available at the end of the article

Graphical Abstract

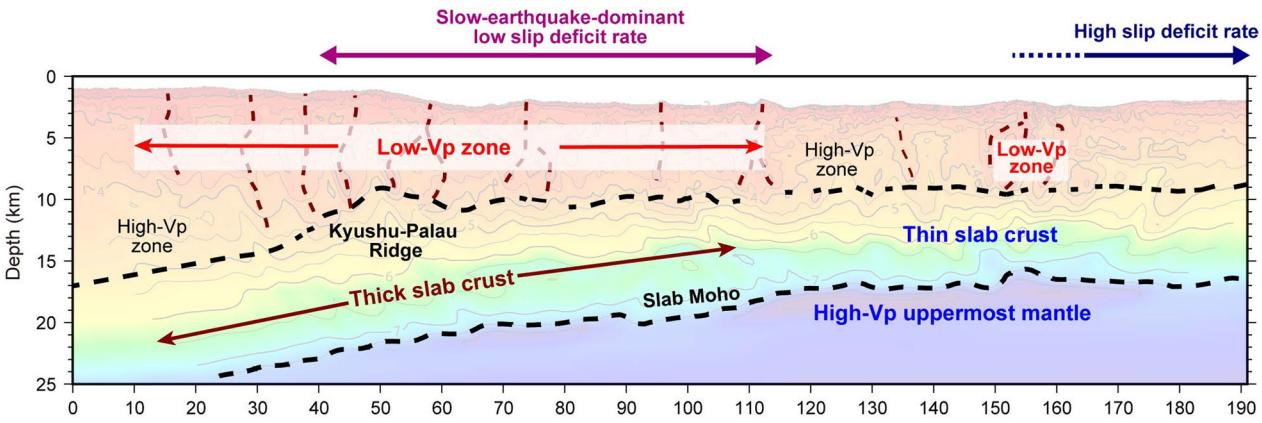

Introduction

Delimiting seismogenic zones at megathrust faults is a crucial step for assessing seismic and tsunami hazards that occur in subduction zones. Observational studies for megathrust earthquakes over the last several decades have documented that the rupture propagation and termination are significantly affected by along-strike variations in frictional and mechanical properties at the fault plane that are linked to upper-plate and lower-plate structural heterogeneities (Sparkes et al. 2010; Bassett et al. 2016; Arnulf et al. 2022). Among various controlling factors, fault roughness or topographic reliefs on subducting plates, in particular, have been the focus of intensive discussion on complex seismic slip behaviors (Bassett and Watts 2015; Bangs et al. 2023). While early studies postulated that seamounts are apt to serve as strongly coupled regions when subducted by increasing the normal stress acting on their upper surface (Scholz and Small 1997), it has been increasingly suggested that seamounts tend to retard large earthquake slip by deflecting or inhibiting coseismic rupture along the plate interface (Kodaira et al. 2000; Mochizuki et al. 2008; Wang and Bilek 2014; Geersen et al. 2015). In addition, seamounts are most likely to leave distinctive but complicated patterns of deformation in the overriding plate during subduction that result in tectonic erosion (Bangs et al. 2006), forearc uplift (Sak et al. 2009), trough embayment (von Huene 2008), conjugate fault development (Davidson et al. 2020) and formation of permeable fracture networks (Arai et al. 2023).

The Nankai Trough, SW Japan, is one of the best locations to study structural controls on seismogenic processes associated with seamount subduction. The Nankai subduction zone has historically hosted recurring megathrust earthquakes with a magnitude of greater than 8 (Ando 1975), and consequently holds high probability to cause equivalent earthquakes in future (Fukushima et al. 2023). The westernmost part of the seismogenic zones lies in a particularly complex tectonic setting (Fig. 1). The structure of the incoming Philippine Sea plate varies from oceanic lithosphere constituting the Shikoku basin in the east to the remnant arc named the Kyushu-Palau ridge in the west (Nishizawa et al. 2016). Coinciding with this structural difference is a major along-trough variation in the strength of interplate locking. While the area off Cape Ashizuri has high slip deficit rates (Yokota et al. 2016) and is thought to have been a primary seismic and tsunami source area during the megathrust earthquake in 1946 (Baba and Cummins 2005), the plate coupling rapidly becomes weak to the west as it approaches the Hyuga-nada area where the Kyushu-Palau ridge is subducting (Wallace et al. 2009; Yokota et al. 2016; Fig. 1). The spatial change in plate coupling is also exemplified by the distribution of low-frequency tremors (Yamashita et al. 2021), very low-frequency earthquakes (Baba et al. 2020) and potential shallow slow slip events (Yokota and Ishikawa 2020; Okada et al. 2022) (Fig. 1).

A seismic investigation in the Hyuga-nada area by Arai et al. (2023) discovered upper-plate low-velocity columns that extend almost vertically from near seafloor to the plate boundary at 10–13 km depths. The results demonstrated that the kilometer-wide fracture zones in the upper plate, interpreted as potential fluid conduits, are linked to the source areas of low-frequency tremor distributed above and around the subducting Kyushu-Palau ridge (Arai et al. 2023). However, the eastern limit of the upper-plate low-velocity zones was not defined in the study, and its relation

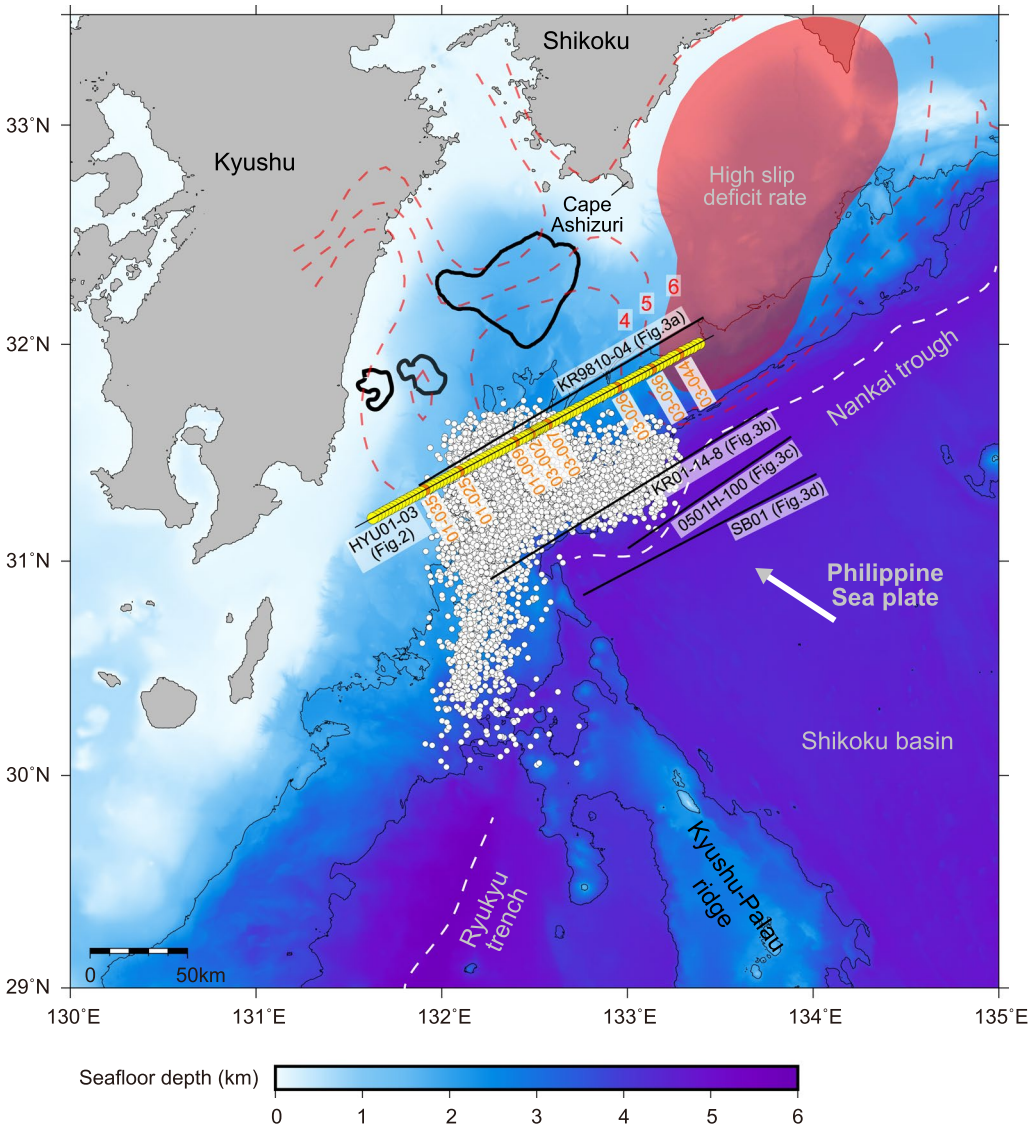

Fig. 1 Bathymetric map showing tectonic setting and survey layouts. Colored circles and a thin black line indicate the OBS locations of the HYU01-03 profile and air-gun shots used in this study. Waveform records of OBSs marked by orange circles are shown in Supporting Information. Solid black lines are the locations of MCS reflection profiles (Fig. 3). White dots denote epicenters of low-frequency tremors (Yamashita et al. 2015, 2021). Red dashed contours with a shade indicate the slip deficit rate at the plate interface (in centimeter per year) (Yokota et al. 2016). Thick black curves outline the source areas of historical interplate earthquakes (Yagi et al. 1998, 2001). The white arrow is the plate motion of the Philippine Sea plate relative to the overriding plate (Miyazaki and Heki 2001)

to the along-trough change in plate coupling is yet to be examined. In addition, causes of the extensive distribution of the upper-plate low-velocity zones that are significantly larger than the apparent width of the Kyushu-Palau ridge remain unexplained. In the present study, we extend the seismic profile of Arai et al. (2023) further east to cover the aforementioned transitional area of the plate coupling condition in the westernmost Nankai trough (Fig. 1). We analyze seismic refraction/wide-angle reflection data by using a full-waveform inversion (FWI) technique to provide high-resolution seismic velocity constraints on both the forearc wedge and the subducting slab. We also examine the existing seismic reflection data focused on the along-trough variation of the incoming plate. The results suggest structural controls on the spatial change in interplate slip mode and thus provide important implications on the western limit of future megathrust earthquakes in the Nankai Trough.

Seismic data

We performed a series of active-source seismic experiments in the forearc region of the westernmost Nankai Trough. We collected seismic refraction/wide-angle reflection data on the along-strike line across the Hyuganada area (HYU01 profile) in 2020, and carried out another seismic survey on the eastern extension of the HYU01 profile with the same specification (HYU03 profile) in 2021. On the HYU01-03 line, a total of 101 ocean bottom seismographs (OBSs) were deployed with 2 km spacing (1 km spacing on the ~ 10-km overlapped section) and recorded the seismic signals generated from tuned air-gun arrays with a volume of 10,600 cubic inches (Figs. 1 and S1–S8). The shot spacing was 200 m. While the data from the western profile (HYU01 profile) were processed in our previous study (Arai et al. 2023), we incorporate the eastern HYU03 data into the present analyses to create seismic velocity models of a ~ 200-km-long transect. The dense coverage from this long seismic profile is well suited to examine the regional architecture associated with ridge subduction.

The analyses for the OBS data followed the procedure of Arai et al. (2023). After locating OBSs using direct water arrivals, we first applied traveltime tomographic inversion to manually picked first arrivals to constrain P-wave velocity (Vp) with large-scale heterogeneities (Figure S9). For this analysis, we used 57,535 first arrivals. The root-mean-squared traveltime misfit was reduced from 1.07 to 0.06 s after 13 iterations. The final inversion result was resampled to 40 m grid spacings and then used as the initial Vp model of the subsequent FWI analysis. In the FWI analysis, the bottom of the Vp model was set at 25 km depth, 2 km deeper than that in the previous study of Arai et al. (2023), to sufficiently capture the structural characteristics of the slab. We performed two-dimensional, frequency-domain, acoustic FWI using TOY-2DAC, a FWI code developed by SEISCOPE (Métivier and Brossier 2016; Górszczyk et al. 2017). The initial model of density structure was prepared by converting the Vp values based on the first-arrival tomography using the Gardner's relationship (Gardner et al. 1974). We also employed Vp-dependent Q values to take the effect of seismic attenuation into account. To improve stability and convergence of the inversion, we started the calculation from a low-frequency range of 2.5–3.5 Hz and progressively included higher frequency components up to 7.5 Hz. Additional information regarding the OBS data processing is presented in Arai et al. (2023) and Supporting Information file (Figures S1–S10 and Table S1).

Seismic reflection data were also acquired on the HYU01-03 profile during the seismic experiments in 2020 and 2021 (Fig. 1). We used the same air-gun system as the OBS refraction surveys and fired every 50 m. A 5.6-km-long streamer cable with 444 channels was towed at 25 m depth below the sea level. The processing of these reflection data was conducted by DownUnder GeoSolutions (DUG). Same as the preceding study (Arai et al. 2023), a sequence of processing including tidal static correction, swell-noise attenuation, deghosting, source signature deconvolution, surface-related multiples suppression and radon transform filtering was applied to the data to reduce noise and multiple reflections. Then velocity analyses and pre-stack Kirchhoff depth migration were performed to produce the final depth image. The Vp information derived from the OBS refraction data was referred to guide the velocity analysis.

We also examined legacy seismic reflection data on four additional lines that are close to and near parallel to the HYU01–03 profile (Fig. 1). The reflection data were acquired on each line using different parameters, which are summarized in the Supporting Information file (Table S2). The KR9810-4 profile, north of the HYU01-03 line, was analyzed through the same flow as the HYU01-03 reflection data to produce the final depth migrated image. The KR0114-08 profile runs in the proximity of the deformation front along the Nankai Trough (Park et al. 2009), and the remaining two lines, NT0501H and SB01, are located seaward of the trough. We use post-stack time migrated sections of these reflection data to characterize the basement roughness of the incoming Philippine Sea plate.

Results

Vp structure

Our FWI analysis for the OBS refraction data constrains extensive velocity structure in the western Nankai Trough. One of the most important observations is the variability in upper-plate crustal velocity (Fig. 2). The final Vp image reveals that above the plate interface that can be inferred from the reflection image (Fig. 2e), the upper plate exhibits significantly low Vp (below 4.0 km/s) from the seafloor to the depth of the plate interface regionally in the southwestern portion of the profile (10–115 km distance in Fig. 2b) and locally over a narrow 15 km wide zone in the northeast (145–160 km distance). The upper-plate heterogeneities are illuminated more clearly in the plot of the Vp perturbation from the one-dimensional depth average (depth below seafloor), which shows that several low-velocity zones develop almost vertically from shallow to over 10 km depth (Fig. 2c). Adjacent to the primary low-velocity portions is a high-velocity body whose velocities are over 1.0 km/s higher than the low-velocity parts at the same depth (115–145 km distance in Fig. 2b). The easternmost part of the model also exhibits higher velocities and likely includes laterally extending low-velocity layers (160–191 km distance in Fig. 2b).

The background lithology of the low- and high-velocity bodies remains unknown, but the variation in seismic velocity may reflect the differences in rock composition, degree of fracturing and fluid amount.

The structure of the subducting Philippine Sea plate shows significant along-trough variations in a similar manner to the upper plate. The crustal thickness estimated by the velocity structure (approximated by the thickness of Vp with 5.2–7.5 km/s) is 7–10 km in the southwestern part of the profile (30–110 km distance in Fig. 2b and d), which is 2–4 km greater than the oceanic crust with a typical thickness of 5–6 km further northeast (110–170 km distance in Fig. 2d). In addition, Vp at the uppermost slab mantle also varies laterally. While the maximum Vp values below the thicker crust of the slab in the southwest is around 8.0 km/s, the mantle velocity beneath the thinner crust to the northeast is significantly higher and exceeds 8.5 km/s. It is noted that these laterally contrasting structures in the subducting slab are consistent with the structural transition from low to high velocities in the upper plate (at 110 km distance in Fig. 2b and c). In other words, the region of thicker crust underlies the upper-plate low-velocity features over a at least 80 km length (30–110 km distance in Fig. 2b and d). Ray coverage of first-arrival refraction waves and the results of checkerboard resolution tests demonstrate that all these features are well constrained by the data (Figure S10).

MCS reflection images

Seismic reflection data provide detailed information on the geometry of structural interfaces. The reflection image along the HYU01–03 profile reveals reflective zones at 8–15 km depth that we interpret as underthrust sediments and/or the upper surface of the slab basement (Fig. 2e). The reflective zone is mostly continuous over the whole profile, but it shows some spatial variations. The most outstanding feature is a ridge-shaped structure with a ~ 2 km relative height in the southwestern part (40–60 km distance in Fig. 2e), which is interpreted as the subducted Kyushu-Palau ridge. Southwest of the ridge, reflection phases for the plate boundary are very weak (0–40 km distance in Fig. 2e). Northeast of the ridge the reflectivity becomes variable and is significantly reduced at some locations (75–80 km and 110–115 km distance in Fig. 2e). In the northeasternmost part of the profile, on the other hand, the reflectors become smoother and more continuous (135–190 km distance in Fig. 2e). We find a similar and more obvious rough-to-smooth transition in plate boundary geometry along the KR9810-4 profile (Fig. 3a). Despite the proximity to the HYU01-03 profile, the reflection image along the KR9810-04 profile shows the rougher plate geometry in the southwest probably because this line is located closer to the deeper seamount indicated by a positive magnetic anomaly (Fig. 4b) while the HYU01-03 profile runs between the shallow and deep seamounts.

Along-trough variability in basement roughness of the incoming plate can be also observed in reflection images on the seaward side of the trough. The reflection data consistently show that there are abundant basement highs with a width of a few kilometers on the eastern flank of the Kyushu Palau ridge (Fig. 3b–d). Their relative heights are variable and reach ~ 1 s in two-way traveltime (roughly equivalent to 2 km) at maximum. Importantly, these basement highs are distributed within ~ 60 km distance from the eastern margin of the Kyushu-Palau ridge, and the deeper extension of this location corresponds well with the rough-to-smooth transition observed in the KR9810-04 (red dashed lines in Fig. 3). It is also noted that on the seaward side of the trench, the topographic highs are mostly buried within the sedimentary layers beneath the Shikoku basin. In contrast, the surface of the basement becomes much smoother further east where thick sediments of over 1 s pile up on the oceanic basement (Fig. 3b–d).

Discussion

Our previous study revealed that there exist low-velocity features above the subducting Kyushu-Palau ridge (Arai et al. 2023). The new results presented in this study demonstrate that the forearc low-velocity features develop over a ~ 100 km length along trough, and underthrusting this zone is crust with up to 10 km thickness and a rough surface together with the main body of the Kyushu-Palau ridge (Figs. 2 and 4c). This observation indicates that the along-trough extent of the upper-plate low-velocity areas is tens of kilometers larger than the width of the

(See figure on next page.)

Fig. 2 Interplate coupling, tremor distribution and seismic structure along the HYU01-03 profile. **a** Tremor frequency by Yamashita et al. (2015) (solid blue line) and Yamashita et al. (2021) (dashed light-blue line) and slip deficit rate by Yokota et al. (2016) (red curves). The numbers of tremors that occurred within 5-km distance from the seismic line are projected. **b** P-wave (Vp) velocity model by full-waveform inversion. The black dashed line is the plate boundary inferred from the MCS reflection image in panel (**e**). Areas without ray coverage of first-arrival refraction waves or poor checkerboard recovery are shaded (Figure S10). **c** Vp perturbation from the depth average of the Vp model (depth below seafloor). **d** Variation in crustal thickness of the subducting Philippine Sea plate approximated by the vertical thickness of areas with Vp of 5.2–7.5 km/s. **e** Pre-stack depth migrated reflection image that highlights the along-profile variation of plate boundary reflections

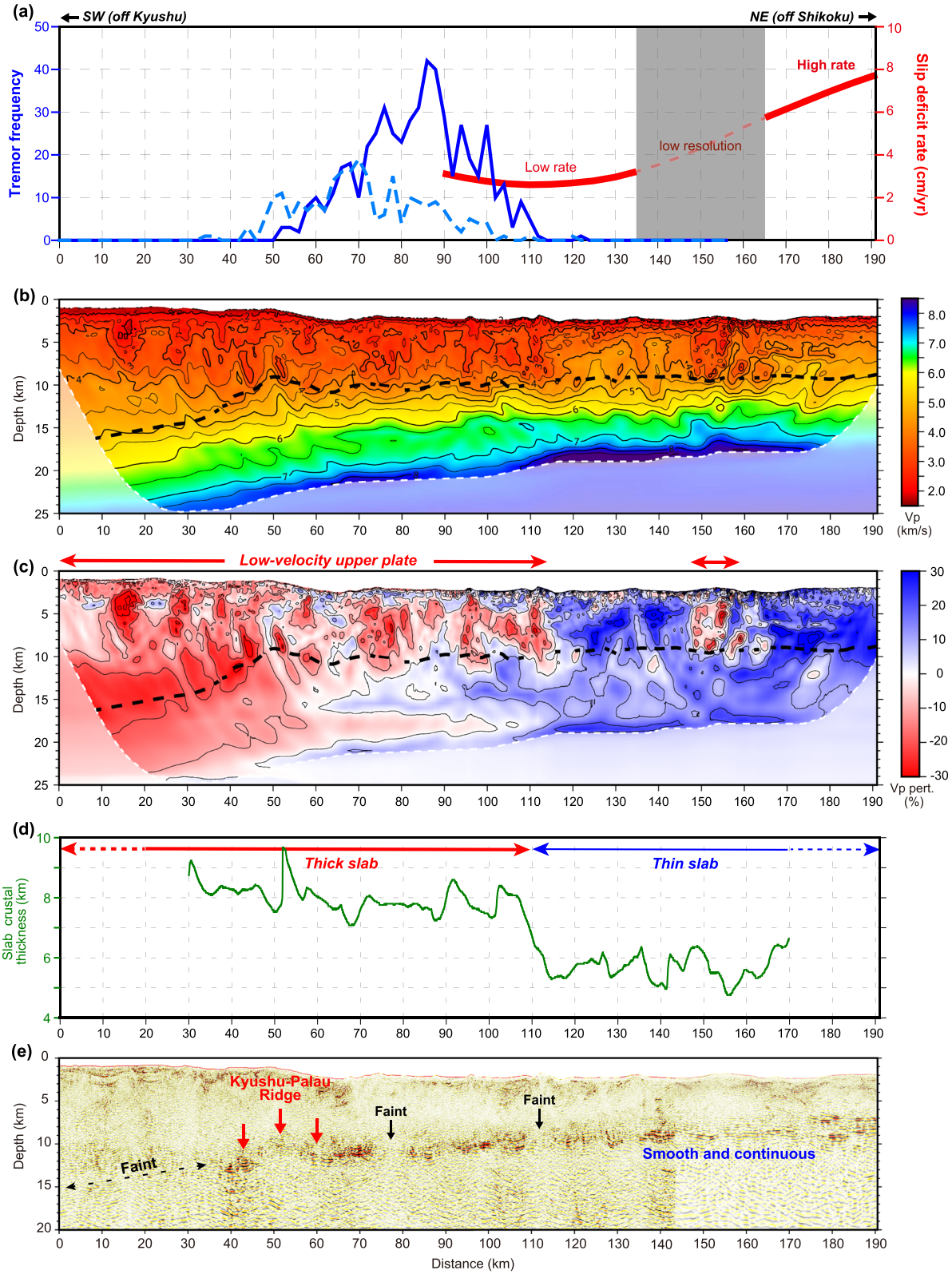

Fig. 2 (See legend on previous page.)

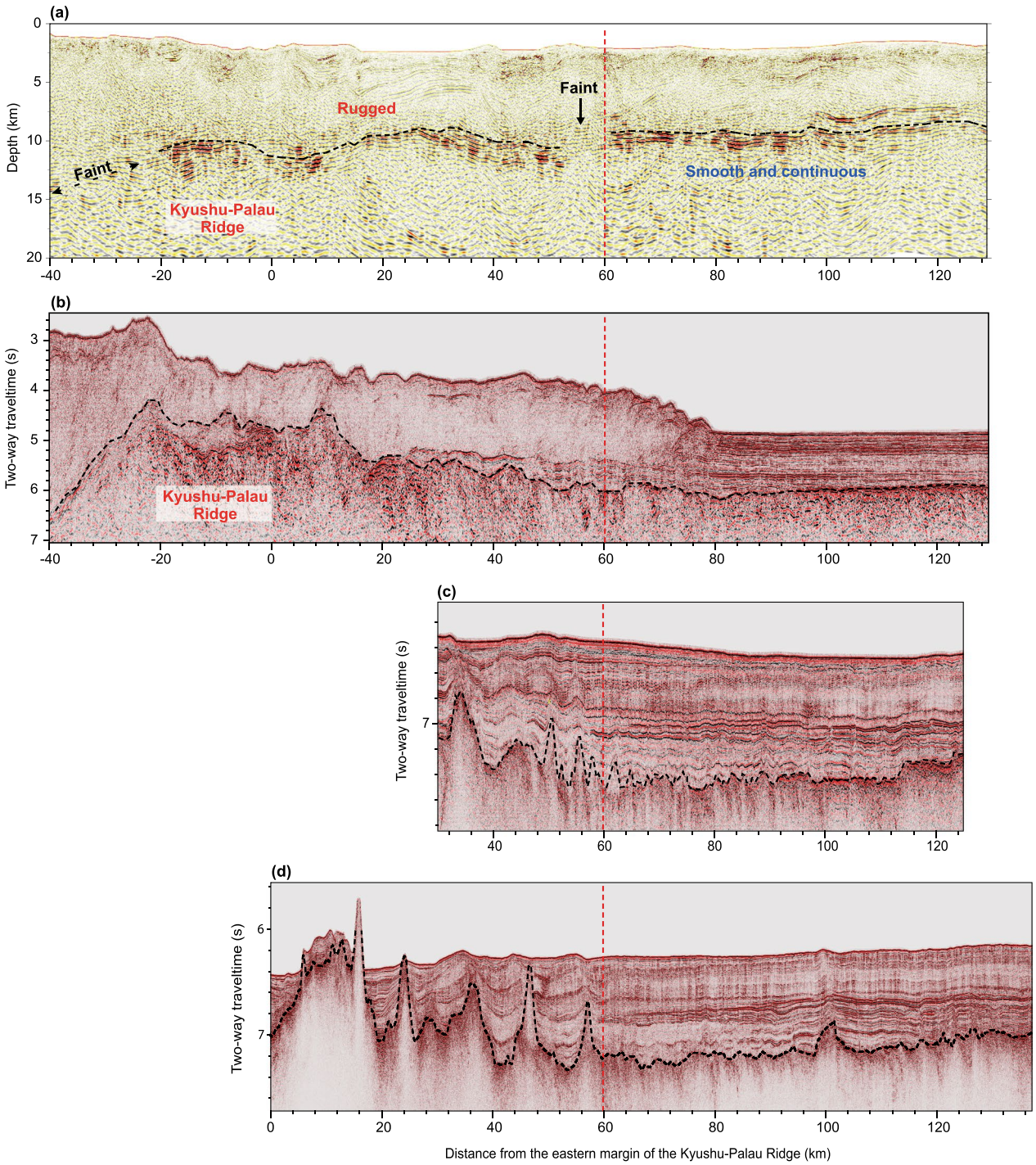

Fig. 3 Seismic reflection images that focus on the along-trough variation in roughness of the incoming plate basement (black dashed lines). **a** KR9810-04. **b** KR01-14-8. **c** 0501H-100. **d** SB01. The red dashed lines mark the transition from the rough basement adjacent to the Kyushu-Palau Ridge to the smooth and continuous basement to the east. Uninterpreted sections are presented in Figure S11

subducted Kyushu-Palau ridge inferred from seafloor magnetic data (Okino 2015; Fig. 4b) and previous seismic studies (Park et al. 2009; Yamamoto et al. 2013). The spatial correlation between the upper-plate and lower-plate structural heterogeneities suggests that the topographic highs on the incoming basement are responsible for the formation of the upper-plate low-velocity features. Numerical studies reproducing the processes of forearc

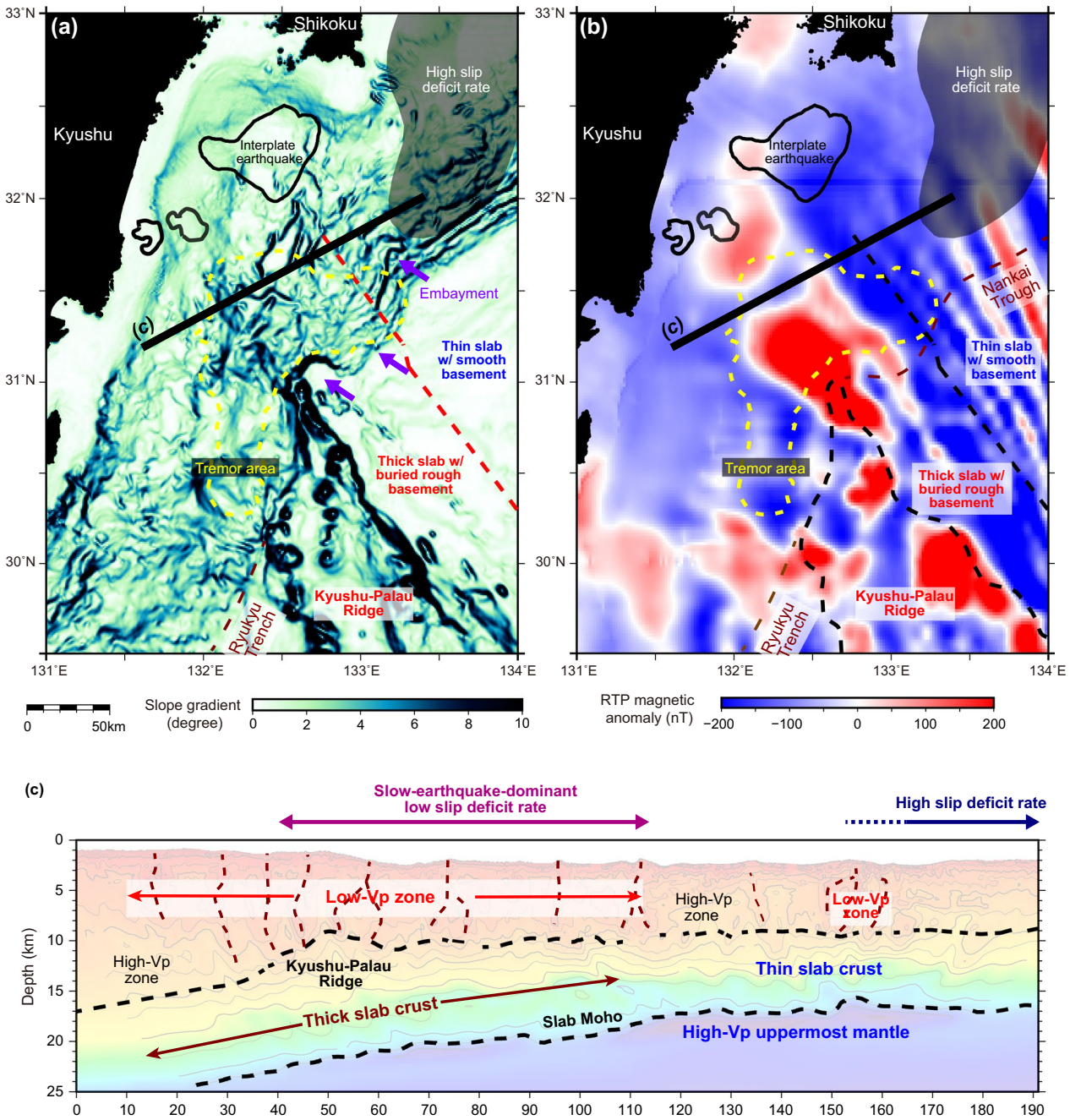

Fig. 4 **a** Map of seafloor slope gradient highlighting the seafloor morphology of the incoming plate and the embayment structures of the trough axis (purple arrows). The black dashed line indicate the boundary between the rough basement adjacent to the Kyushu-Palau Ridge to the smooth and continuous basement to the east (Fig. 3). **b** Map of the reduced-to-pole (RTP) magnetic anomaly (Okino 2015; Arai et al. 2023) showing the transition from positive anomalies corresponding to the Kyushu-Palau ridge to the easterly Shikoku basin with linear alternating patterns. **c** Cartoon interpretations of the HYU01-03 Vp model

deformation associated with seamount subduction demonstrate that even small-scale bumps on the incoming plate are capable for uplifting the forearc wedge and causing intensive fractures above the basement highs (Morgan and Bangs 2017; Miyakawa et al. 2022). As observed in the bathymetric map of the Hyuga-nada area, the forearc slope exhibits complicated patterns of deformation, and the trough axis is highly indented and includes embayment structure at some locations to the east of the Kyushu-Palau ridge (Fig. 4a). The smaller low-Vp

zone (145–160 km distance in Fig. 2c) corresponds well with the downdip extension of the embayment labeled in Fig. 4a. Based on sandbox experiments, Dominguez et al. (1998) demonstrate that seamounts can induce intensive fracture zones consisting of subvertical faults within the overriding plate in the process of subduction. We thus suggest that not only the main body of the Kyushu-Palau ridge, but also the anomalously thick and rough crustal portion developed in its eastern flank contribute to forming regional low-velocity zones in the overriding plate.

Along-trough structural variations mentioned above closely correlate with spatial changes in interplate slip mode along the Nankai subduction zone. The comparison with tremor distribution (Yamashita et al. 2015, 2021; Fig. 2a) shows that the slow earthquakes are limited in the areas where the plate boundary is reflective and the upper-plate Vp values are below 4.5 km/s (40–115 km distance in Fig. 2). The slip deficit rate determined by seafloor geodetic observation (Yokota et al. 2016) also transitions from low in the middle of the profile to high in the easternmost part in concert with a change in upper-plate velocity structure (Fig. 2a). These results indicate that the subducting Kyushu-Palau ridge and the adjacent portion with thicker crust and rough basement can weaken the plate coupling. It is widely recognized that subducting seamounts facilitate local underthrusting of fluid-rich sediments along their trails (Bangs et al. 2023). These sediments prepare preferable conditions for shallow slow earthquakes to occur by expelling fluids and creating zones with high pore fluid pressure at/around the plate interface (e.g., Akuhara et al. 2020). In addition, the low-velocity upper plate damaged by subducting seamount has reduced rigidity, which may hamper the sustained strain accumulation that is necessary for large megathrust earthquakes (Sallarès and Ranero 2019; Bassett et al. 2022). From another viewpoint, the incoming Philippine Sea plate has a significant along-trough variation in thickness of trench sediments around the Kyushu-Palau ridge (Fig. 3). This may be also relevant because thick incoming sediments likely result in larger rupture areas of megathrust earthquakes by smoothing out the potential fault plane and decreasing the dip angle of the slab (Bletery et al. 2016; Brizzi et al. 2020). In the study area, the trench sediments tend to be thicker to the east (south off the Cape Ashizuri) where the slip deficit rate is higher (Fig. 3). Park and Jalami Hondori (2023) investigated seismic reflection data along the entire Nankai trough to suggest that the distribution of the underplating turbidite layers within the Shikoku Basin sediments have a positive correlation with the offshore areas with high slip deficit rates, which agrees with our observations in the Hyuganada area that the Shikoku Basin sediments become thinner or missing as it approaches the Kyushu-Palau ridge (Fig. 3b–d). These correlations between the plate coupling, upper-plate seismic velocity and incoming plate structure are also consistent with those observed in other subduction zones. For example, the Hikurangi margin, situated off the east coast of New Zealand's North Island, exhibits a similar lateral change in interplate coupling that is closely linked to the variation in upper-plate forearc velocity (Bassett et al. 2022). It has been also suggested that the variations in sediment thickness and topography of the incoming Hikurangi Plateau contribute to developing the variable slip mode along the plate interface (Gase et al. 2022; Bassett et al. 2023). We thus suggest that the combination of these structural factors primarily controls the complex spatial pattern of seismogenic behaviors in the western Nankai Trough.

Although the along-trough structural variation of the incoming Philippine Sea plate is revealed in this study, the tectonic processes on how the thick crust with rugged basement surface has developed in the eastern flank of the Kyushu-Palau ridge are still unclear. The Kyushu–Palau ridge located west of the Shikoku and Parece Vela basins is a remnant arc that had separated from the Izu-Bonin-Mariana arc on the eastern side of the basins through back-arc rifting and spreading (Okino et al. 1999). Seismic refraction surveys of Nishizawa et al. (2016) show that the northern Kyushu-Palau ridge has an 18-km-thick crust and accompanies a transitional zone on its eastern side. Although the transitional zone has a rough basement surface similar to those observed in this study, they observed highly thinned crust with ~ 5 km thickness in the transitional zone resulted from arc and back-arc rifting, which differs from the thick slab crust found in this study. Another seismic study focused on the southern part of the Kyushu-Palau ridge indicate that the crust in the transitional zone has a thickness of ~ 10 km, which is equivalent to the values from this study, and argue that extensive arc and back-arc volcanisms may have contributed to crustal thickening (Zhang et al. 2023). The alternative model is anomalously thick "oceanic" crust that was created at back-arc spreading centers: if the back-arc spreading centers are located close to the volcanic arc at an initial stage of back-arc spreading, slab-derived fluids may be supplied abundantly to the spreading axes, resulting in anomalous crust with 8–10 km thickness (Arai and Dunn 2014). Seafloor magnetic data show weak linear patterns aligned perpendicular to the spreading direction just east of the Kyushu-Palau Ridge, which implicitly indicates that the transitional zone is composed of oceanic crust formed through back-arc spreading (Fig. 4b). In either case, thicker crust can be more buoyant than typical oceanic

crust and thus may have more impacts on the upper-plate deformation when subducted (Arai et al. 2017).

Conclusions

We investigated the along-trough structural variations in the upper-plate forearc and the subducting slab in the western Nankai Trough using seismic refraction data recorded by densely deployed OBSs and MCS reflection data. We constrained P-wave velocity structure of the ~ 200-km-long transect with the high resolution by using the full-waveform inversion technique and revealed that the upper plate shows low seismic velocities over an approximately 100 km length that coincide with the location of predominant occurrence of slow earthquakes. Furthermore, we observed that the upper-plate low-velocity zone is underthrust by the slab with 2–4 km thicker crust that has substantial basement irregularities spanning ~ 60 km from the eastern end of the Kyushu-Palau ridge beneath the Shikoku basin. We propose that combined influences of this thicker and rugged slab crust and the adjacent mature arc of the Kyushu-Palau ridge can induce significant fracture zones in the overriding plate, reduce the interplate coupling and provide favorable conditions for the occurrence of shallow slow earthquakes.

Supplementary Information

The online version contains supplementary material available at https://doi.org/10.1186/s40623-024-02025-4.

Supplementary Material 1. Figure S1. a OBS records, b synthetic seismograms from the full waveform inversion (FWI) Vp model and c synthetic seismograms from the first arrival tomography (FAT) Vp model of OBS at HYU03-s044. Figure S2. a OBS records, b synthetic seismograms from the FWI Vp model and c synthetic seismograms from the FAT Vp model of OBS at HYU03-s036. Figure S3. a OBS records, b synthetic seismograms from the FWI Vp model and c synthetic seismograms from the FAT Vp model of OBS at HYU03-s026. Figure S4. a OBS records, b synthetic seismograms from the FWI Vp model and c synthetic seismograms from the FAT Vp model of OBS at HYU03-s007. Figure S5. a OBS records, b synthetic seismograms from the FWI Vp model and c synthetic seismograms from the FAT Vp model of OBS at HYU03-s002. Figure S6. a OBS records, b synthetic seismograms from the FWI Vp model and c synthetic seismograms from the FAT Vp model of OBS at HYU01-s035. Figure S7. a OBS records, b synthetic seismograms from the FWI Vp model and c synthetic seismograms from the FAT Vp model of OBS at HYU01-s025. Figure S8. a OBS records, b synthetic seismograms from the FWI Vp model and c synthetic seismograms from the FAT Vp model of OBS at HYU01-s009. Figure S9. a Initial Vp model for first arrival tomography (FAT). Black dots indicate OBS locations. b Result of FAT that is used as the initial model of the full waveform inversion (FWI). c Final Vp model of FWI. Figure S10. a Ray coverage of refraction waves in FAT. Checkerboard resolution tests of FWI with velocity anomaly size of 3 × 3 km (b) and 1 × 1 km (c). Based on the results, the area above the white/black dashed line is interpreted for discussion (Figure 2). Figure S11. Uninterpreted seismic reflection images. a KR9810-04. b HYU01-03. c KR01-14-8. d 0501H-100. e SB01. Table S1. FWI parameters and reduction in cost function at each inversion step. Table S2. Seismic data acquisition parameters.

Acknowledgements

We thank the captains, crews and marine technicians onboard the JAMSTEC research vessels Kaimei, Kairei and Yokosuka for their operations during the cruises of KM21-07, KM20-05, KR20-10, YK21-14 and YK21-19. Figures were created using the Generic Mapping Tools version 6 (Wessel et al. 2019). Comments from Demian Saffer, Tianhaozhe Sun and Ryota Hino were helpful to improve the quality of the manuscript. We are also grateful for constructive reviews by Rebecca Bell and an anonymous reviewer.

Author contributions

R. A. analyzed the seismic data and drafted the manuscript. K. S., Y. N., S. M. and T. T. contributed to seismic data acquisition as chief scientists of each cruise. G. F., S. K. and K. M. managed the project and supervised the data acquisition and processing. D. B. processed the legacy MCS reflection data and interpreted the results. Y. K. and Y. Ham. participated in the seismic cruise. R. N., M. K. and Y. Has. led the acquisition and processing of the MCS reflection data. K.O. analyzed and interpreted the seafloor magnetic data. All the authors contributed to scientific discussions.

Funding

This study was supported by the Japan Society for the Promotion of Science KAKENHI (Grant Number JP22K03789, JP21H05202 and 16H06475).

Availability of data and materials

Seismic data presented in this study are available through JAMSTEC Seismic Survey Database Site (https://doi.org/https://doi.org/10.17596/0002069).

Declarations

Competing interests

We declare no competing interests.

Author details

[1]Research Institute for Marine Geodynamics, Japan Agency for Marine-Earth Science and Technology, 3173-25 Showa-machi Kanazawa-ku, Yokohama, Kanagawa 236-0001, Japan. [2]GNS Science, 1 Fairway Drive, Avalon 5011, PO Box 30368, Lower Hutt 5040, New Zealand. [3]Kochi Institute for Core Sample Research, Japan Agency for Marine-Earth Science and Technology, 200 Monobe Otsu Nankoku, Kochi 783-8502, Japan. [4]Earthquake Research Institute, The University of Tokyo, 1-1-1 Yayoi Bunkyo-ku, Tokyo 113-0032, Japan. [5]Lawrence Berkeley National Laboratory, 1 Cyclotron Road, Berkeley, CA 94720, USA. [6]Faculty of Science and Technology, Kochi University, Akebonocho 2-5-1, Kochi 780-8520, Japan. [7]Atmosphere and Ocean Research Institute, The University of Tokyo, 5-1-5 Kashiwanoha Kashiwa, Chiba 277-8564, Japan.

Received: 12 March 2024 Accepted: 7 May 2024
Published online: 15 May 2024

References

Akuhara T, Tsuji T, Tonegawa T (2020) Overpressured underthrust sediment in the Nankai Trough forearc inferred from transdimensional inversion of high-frequency teleseismic waveforms. Geophys Res Lett 47:e2020GL088280. https://doi.org/10.1029/2020GL088280

Ando M (1975) Source mechanisms and tectonic significance of historical earthquakes along the Nankai trough, Japan. Tectonophysics 27:119–140. https://doi.org/10.1016/0040-1951(75)90102-X

Arai R, Dunn R (2014) Seismological study of Lau back arc crust: mantle water, magmatic differentiation, and a compositionally zoned basin. Earth Planet Sci Lett 390:304–317. https://doi.org/10.1016/j.epsl.2014.01.014

Arai R, Kodaira S, Yamada T, Takahashi T, Miura S, Kaneda Y, Nishizawa A, Oikawa M (2017) Subduction of thick oceanic plateau and high-angle normal-fault earthquakes intersecting the slab. Geophys Res Lett 44:6109–6115. https://doi.org/10.1002/2017GL073789

Arai R, Miura S, Nakamura Y, Fujie G, Kodaira S, Kaiho Y, Mochizuki K, Nakata R, Kinoshita M, Hashimoto Y, Hamada Y, Okino K (2023) Upper-plate conduits linked to plate boundary that hosts slow earthquakes. Nat Comm 14:5101. https://doi.org/10.1038/s41467-023-40762-4

Arnulf AF, Bassett D, Harding AJ, Kodaira S, Nakanishi A, Moore G (2022) Upper-plate controls on subduction zone geometry, hydration and earthquake behaviour. Nat Geosci 15:143–148. https://doi.org/10.1038/s41561-021-00879-x

Baba T, Cummins PR (2005) Contiguous rupture areas of two Nankai Trough earthquakes revealed by high-resolution tsunami waveform inversion. Geophys Res Lett 32:L08305. https://doi.org/10.1029/2004GL022320

Baba S, Takemura S, Obara K, Noda A (2020) Slow earthquakes illuminating interplate coupling heterogeneities in subduction zones. Geophys Res Lett 47:e2020GL088089. https://doi.org/10.1029/2020GL088089

Bangs NLB, Gulick SPS, Shipley TH (2006) Seamount subduction erosion in the Nankai Trough and its potential impact on the seismogenic zone. Geology 34:701–704. https://doi.org/10.1130/G22451.1

Bangs NL, Morgan JK, Bell RE, Han S, Arai R, Kodaira S, Gase AC, Wu X, Davy R, Frahm L, Tilley HL, Barker DHN, Edwards JH, Tobin HJ, Reston TJ, Henrys SA, Moore GF, Bassett D, Kellett R, Stucker V, Fry B (2023) Slow slip along the Hikurangi margin linked to fluid-rich sediments trailing subducting seamounts. Nat Geosci 16:505–512. https://doi.org/10.1038/s41561-023-01186-3

Bassett D, Watts AB (2015) Gravity anomalies, crustal structure, and seismicity at subduction zones: 1. Seafloor roughness and subducting relief. Geochem Geophys Geosyst 16:1508–1540. https://doi.org/10.1002/2014GC005684

Bassett D, Sandwell DT, Fialko Y, Watts AB (2016) Upper-plate controls on co-seismic slip in the 2011 magnitude 9.0 Tohoku-oki earthquake. Nature 531:92–96. https://doi.org/10.1038/nature16945

Bassett D, Arnulf A, Henrys S, Barker D, van Avendonk H, Bangs N, Kodaira S, Seebeck H, Wallace L, Gase A, Luckie T, Jacobs K, Tozer B, Arai R, Okaya D, Mochizuki K, Fujie G, Yamamoto Y (2022) Crustal structure of the Hikurangi margin from SHIRE seismic data and the relationship between forearc structure and shallow megathrust slip behavior. Geophys Res Lett 49:e2021GL096960. https://doi.org/10.1029/2021gl096960

Bassett D, Fujie G, Kodaira S, Arai R, Yamamoto Y, Henrys S, Barker D, Gase A, van Avendonk H, Bangs N, Seebeck H, Tozer B, Jacobs K, Luckie T, Okaya D, Mochizuki K (2023) Heterogeneous crustal structure of the Hikurangi Plateau revealed by SHIRE seismic data: Origin and implications for plate boundary tectonics. Geophys Res Lett 50:e2023GL105674. https://doi.org/10.1029/2023GL105674

Bletery Q, Thomas AM, Rempel AW, Karlstrom L, Sladen A, De Barros L (2016) Mega-earthquakes rupture flat megathrusts. Science 354:1027–1031. https://doi.org/10.1126/science.aag0482

Brizzi S, van Zelst I, Funiciello F, Corbi F, van Dinther Y (2020) How sediment thickness influences subduction dynamics and seismicity. J Geophys Res Solid Earth 125:e2019JB018964. https://doi.org/10.1029/2019JB018964

Davidson SR, Barnes PM, Pettinga JR, Nicol A, Mountjoy JJ, Henrys SA (2020) Conjugate strike-slip faulting across a subduction front driven by incipient seamount subduction. Geology 48:493–498. https://doi.org/10.1130/G47154.1

Dominguez S, Lallemand SE, Malavieille J, von Huene R (1998) Upper plate deformation associated with seamount subduction. Tectonophysics 293:207–224. https://doi.org/10.1016/S0040-1951(98)00086-9

Fukushima Y, Nishikawa T, Kano Y (2023) High probability of successive occurrence of Nankai megathrust earthquakes. Sci Rep 13:63. https://doi.org/10.1038/s41598-022-26455-w

Gardner GHF, Gardner LW, Gregory AR (1974) Formation velocity and density—the diagnostic basics for stratigraphic traps. Geophysics 39:770–780. https://doi.org/10.1190/1.1440465

Gase AC, Bangs NL, Van Avendonk HJ, Bassett D, Henrys SA (2022) Hikurangi megathrust slip behavior influenced by lateral variability in sediment subduction. Geology 50:1145–1149. https://doi.org/10.1130/G50261.1

Geersen J, Ranero CR, Barckhausen U, Reichert C (2015) Subducting seamounts control interplate coupling and seismic rupture in the 2014 Iquique earthquake area. Nat Comm 6:8267. https://doi.org/10.1038/ncomms9267

Górszczyk A, Operto S, Malinowski M (2017) Toward a robust workflow for deep crustal imaging by FWI of OBS data: the eastern Nankai Trough revisited. J Geophys Res Solid Earth 122:4601–4630. https://doi.org/10.1002/2016JB013891

Kodaira S, Takahashi N, Nakanishi A, Miura S, Kaneda Y (2000) Subducted seamount imaged in the rupture zone of the 1946 Nankaido earthquake. Science 289:104–106. https://doi.org/10.1126/science.289.5476.104

Métivier L, Brossier R (2016) The SEISCOPE optimization toolbox: a large-scale nonlinear optimization library based on reverse communication. Geophysics 81:F1–F15. https://doi.org/10.1190/geo2015-0031.1

Miyakawa A, Noda A, Koge H (2022) Evolution of the geological structure and mechanical properties due to the collision of multiple basement topographic highs in a forearc accretionary wedge: insights from numerical simulations. Prog Earth Planet Sci 9:1. https://doi.org/10.1186/s40645-021-00461-4

Miyazaki S, Heki K (2001) Crustal velocity field of southwest Japan: subduction and arc-arc collision. J Geophys Res 106:4305–4326. https://doi.org/10.1029/2000JB900312

Mochizuki K, Yamada T, Shinohara M, Yamanaka Y, Kanazawa T (2008) Weak interplate coupling by seamounts and repeating M~7 earthquakes. Science 321:1194–1197. https://doi.org/10.1126/science.1160250

Morgan JK, Bangs NL (2017) Recognizing seamount-forearc collisions at accretionary margins: insights from discrete numerical simulations. Geology 45:635–638. https://doi.org/10.1130/G38923.1

Nishizawa A, Kaneda K, Oikawa M (2016) Crust and uppermost mantle structure of the Kyushu-Palau Ridge, remnant arc on the Philippine Sea plate. Earth Planets Space 68:30. https://doi.org/10.1186/s40623-016-0407-3

Okada Y, Nishimura T, Tabei T, Matsushima T, Hirose H (2022) Development of a detection method for short-term slow slip events using GNSS data and its application to the Nankai subduction zone. Earth Planets Space 74:18. https://doi.org/10.1186/s40623-022-01576-8

Okino K (2015) Magnetic anomalies in the Philippine Sea: implications for regional tectonics. J Geogr 124:729–747. https://doi.org/10.5026/jgeography.124.729

Okino K, Ohara Y, Kasuga S, Kato Y (1999) The Philippine Sea: new survey results reveal the structure and the history of the marginal basins. Geophys Res Lett 26:2287–2290. https://doi.org/10.1029/1999GL900537

Park JO, Jamali Hondori E (2023) Link between the Nankai underthrust turbidites and shallow slow earthquakes. Sci Rep 13:10333. https://doi.org/10.1038/s41598-023-37474-6

Park JO, Hori T, Kaneda Y (2009) Seismotectonic implications of the Kyushu-Palau ridge subducting beneath the westernmost Nankai forearc. Earth Planets Space 61:1013–1018. https://doi.org/10.1186/BF03352951

Sak PB, Fisher DM, Gardner TW, Marshall JS, LaFemina PC (2009) Rough crust subduction, forearc kinematics, and Quaternary uplift rates, Costa Rican segment of the Middle American Trench. Geology 121:992–1012. https://doi.org/10.1130/B26237.1

Sallarès V, Ranero CR (2019) Upper-plate rigidity determines depth-varying rupture behaviour of megathrust earthquakes. Nature 576:96–101. https://doi.org/10.1038/s41586-019-1784-0

Scholz CH, Small C (1997) The effect of seamount subduction on seismic coupling. Geology 25:487–490. https://doi.org/10.1130/0091-7613(1997)025%3c0487:TEOSSO%3e2.3.CO;2

Sparkes R, Tilmann F, Hovius N, Hillier J (2010) Subducted seafloor relief stops rupture in South American great earthquakes: implications for rupture behaviour in the 2010 Maule, Chile earthquake. Earth Planet Sci Lett 298:89–94. https://doi.org/10.1016/j.epsl.2010.07.029

von Huene R (2008) When seamounts subduct. Science 321:1165–1166. https://doi.org/10.1126/science.1162868

Wallace LM, Ellis S, Miyao K, Miura S, Beavan J, Goto J (2009) Enigmatic, highly active left-lateral shear zone in southwest Japan explained by aseismic ridge collision. Geology 37:143–146. https://doi.org/10.1130/G25221A.1

Wang K, Bilek SL (2014) Invited review paper: fault creep caused by subduction of rough seafloor relief. Tectonophysics 610:1–24. https://doi.org/10.1016/j.tecto.2013.11.024

Wessel P, Luis JF, Uieda L, Scharroo R, Wobbe F, Smith WHF, Tian D (2019) The generic mapping tools version 6. Geochem Geophys Geosyst 20:5556–5564. https://doi.org/10.1029/2019GC008515

Yagi Y, Kikuchi M, Yoshida S, Yamanaka Y (1998) Source process of the Hyuganada earthquake of April 1, 1968 (M_{JMA}7.5), and its relationship to the subsequent seismicity. Zisin 51:139–148. https://doi.org/10.4294/zisin1948.51.1_139

Yagi Y, Kikuchi M, Sagiya T (2001) Co-seismic slip, post-seismic slip, and aftershocks associated with two large earthquakes in 1996 in Hyuga-nada, Japan. Earth Planets Space 53:793–803. https://doi.org/10.1186/BF03351677

Yamamoto Y, Obana K, Takahashi T, Nakanishi A, Kodaira S, Kaneda Y (2013) Imaging of the subducted Kyushu-Palau Ridge in the Hyuga-nada region,

western Nankai Trough subduction zone. Tectonophysics 589:90–102. https://doi.org/10.1016/j.tecto.2012.12.028
Yamashita Y, Yakiwara H, Asano Y, Shimizu H, Uchida K, Hirano S, Umakoshi K, Miyamachi H, Nakamoto M, Fukui M, Kamizono M, Kanehara H, Yamada T, Shinohara M, Obara K (2015) Migrating tremor off southern Kyushu as evidence for slow slip of a shallow subduction interface. Science 348:676–679. https://doi.org/10.1126/science.aaa4242
Yamashita Y, Shinohara M, Yamada T (2021) Shallow tectonic tremor activities in Hyuga-nada, Nankai subduction zone, based on long-term broadband ocean bottom seismic observations. Earth Planets Space 73:196. https://doi.org/10.1186/s40623-021-01533-x
Yokota Y, Ishikawa T (2020) Shallow slow slip events along the Nankai Trough detected by GNSS-A. Sci Adv 6:eaay5786. https://doi.org/10.1126/sciadv.aay5786
Yokota Y, Ishikawa T, Watanabe S, Tashiro T, Asada A (2016) Seafloor geodetic constraints on interplate coupling of the Nankai Trough megathrust zone. Nature 534:374–377. https://doi.org/10.1038/nature17632
Zhang J, Li J, Ding W, Ruan A, Wei X, Tan P (2023) Crustal structure and magmatism of the southern Kyushu-Palau ridge. Tectonophysics 858:229862. https://doi.org/10.1016/j.tecto.2023.229862

Publisher's Note